





**Sensitive spatially resolved magnetometry using a Bose-condensed gas with a bright probe**Naota Sekiguchi , Kosuke Shibata ,\* Aki Torii, Hiroyuki Toda, Ryohei Kuramoto, Daiki Fukuda, and Takuya Hirano   
*Department of Physics, Gakushuin University, Tokyo 171-8588, Japan* (Received 16 September 2020; revised 4 June 2021; accepted 11 October 2021; published 28 October 2021)

We demonstrate a sensitive spatially resolved magnetometer using a spinor Bose-Einstein condensate (BEC) of  $^{87}\text{Rb}$  atoms with increased probe fluence. By performing a probe parameter search using a two-polarization phase contrast imaging technique, we find that the probe-induced atom loss, a major constraint in optical magnetometry with high-density gas, can be reduced. We attain a sensitivity of 5.4(6) mrad for the phase measurement of Larmor precession using a measurement area of  $1.4 \times 10^2 \mu\text{m}^2$  with a probe fluence of  $4.1 \times 10^5 \mu\text{m}^{-2}$ . A dc magnetic field sensitivity of 5.0(4) pT/ $\sqrt{\text{Hz}}$  is attained with a probe fluence of  $3.9 \times 10^5 \mu\text{m}^{-2}$ . The results should contribute to further enhancement of the sensitivity of a BEC magnetometer.

DOI: [10.1103/PhysRevA.104.L041306](https://doi.org/10.1103/PhysRevA.104.L041306)**I. INTRODUCTION**

High-performance magnetometry is of great importance in fundamental research [1] and applications, including materials science, chemistry, biology, and medicine [2–6]. Sensitivities of sub-fT/ $\sqrt{\text{Hz}}$  have been achieved using centimeter-sized optically pumped magnetometers [7,8] and superconducting quantum interference devices (SQUIDs) [9]. Spatial resolution is also an important factor in magnetometry, but there is a trade-off between a high sensitivity and a fine spatial resolution in general. Nanometer spatial resolutions have been reported using single trapped ions with a sensitivity of a few pT/ $\sqrt{\text{Hz}}$  [10] and single nitrogen-vacancy centers in diamond with a sensitivity of a few nT/ $\sqrt{\text{Hz}}$  [11].

A cold atom cloud is a good medium for spatially resolved magnetometry: it offers high sensitivity and a spatial resolution of micrometer scale [12]. The Bose-Einstein condensate (BEC) is a promising candidate for pursuing high magnetic field sensitivity with a micrometer spatial resolution [13] because of a suppressed thermal motion and a long coherence time [14,15]. A magnetically trapped BEC [16] has been successfully employed to measure magnetic fields from solid-state samples [17]. Spatially resolved magnetometers using spinor BECs, produced in an optical trap, have realized sensitivities of approximately 10 pT/ $\sqrt{\text{Hz}}$  [14,18,19].

A dominant obstacle to enhancing the sensitivity of BEC optical magnetometry is a severe signal decay induced by a probe light [18]. Due to this decay, the probe intensity cannot be increased beyond a certain value and the sensitivity is limited by the photon noise contribution  $\propto 1/\sqrt{N_p}$ , where  $N_p$  is the probe photon number. In many cases, the optimal probe intensity for the best sensitivity is upper-bounded by the balance between the photon shot noise contribution and unavoidable spontaneous photon scattering that causes reorientation of atoms [20]. For a dense gas like a BEC, however, the probe light often causes an excessive signal decay due to

light-assisted collisions [21–23] and superradiance [18]. Therefore, conventional BEC magnetometry has operated with much weaker probe intensity [18], due to the severe signal decay induced by the probe light, than the intensity restricted by the spontaneous photon scattering.

In this Letter, we demonstrated optical magnetometry using a BEC of  $^{87}\text{Rb}$  atoms with increased probe fluence. Using a technique of two-polarization phase contrast imaging (TP-PCI), we measured both the atom loss rate and the decay rate of the Larmor precession amplitude simultaneously during the imaging with less affected by systematic fluctuations. We found that the atom loss rate was asymmetric with respect to the sign of the detuning and was reduced at specific red-detuned probe frequencies. The experimental results suggest that the probe-induced atom loss should be mainly due to light-assisted collisions. With an optimal probe, we achieved a precession phase sensitivity of 5.4(6) mrad over a measurement area of  $1.4 \times 10^2 \mu\text{m}^2$ . The magnetic field sensitivity was 5.0(4) pT/ $\sqrt{\text{Hz}}$ .

This work paves the way for significantly improving BEC optical magnetometers, because optical readout is essential in any optical magnetometers and has been the major limitation on sensitivity as mentioned above. We found that suppression of light-assisted collisions by frequency tuning, which has been used in the context of laser cooling [24,25], works for probing a BEC. This has been overlooked, but is very effective as demonstrated here. The technique should be implemented in other magnetometers as well to enhance the sensitivity. The increased probe fluence will lead to significant reduction of the atomic spin quantum noise because of the quantum non-demolition (QND) feature in our measurement. This quantum enhancement is important for further improving the sensitivity because the atomic noise becomes dominant as the probe fluence is increased.

**II. EXPERIMENTAL SETUP AND METHOD**

TPPCI was implemented with the setup schematically depicted in Fig. 1(a). In this setup, the linearly polarized probe

\*shibata@qo.phys.gakushuin.ac.jp

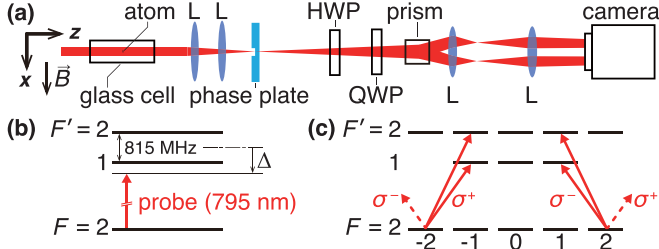


FIG. 1. (a) Illustration of the TPPCI setup. L: lens; HWP: half-wave plate; QWP: quarter-wave plate. (b) Energy diagram of  $^{87}\text{Rb}$  and the frequency of the probe light. (c) Magnetic sublevels. The red solid arrows show allowed transitions.

light, propagating along the  $z$  axis, was decomposed into two circularly polarized components by wave plates and a Nomarski prism. Two polarization components were focused on different regions (regions 1 and 2) of a CCD camera to form phase-contrast images of  $^{87}\text{Rb}$  atoms trapped in an optical dipole trap in a glass cell. These images were used to extract the atom number and spin information, as explained later. The probe light frequency was stabilized with a tunable detuning  $\Delta$  from the  $D_1$  line transition of  $^{87}\text{Rb}$  [see Fig. 1(b)]. The detuning  $\Delta$  was defined with respect to the frequency from the  $F = 2$  state to the center of the excited states  $F' = 1, 2$ . The probe-beam  $1/e^2$  diameter of 3 mm was sufficiently larger than the axial atom-cloud size of  $\sim 90 \mu\text{m}$ .

The atoms were prepared in the hyperfine ground state  $F = 2$  [26]. They were cooled below the critical temperature of Bose-Einstein condensation. The number of atoms was approximately  $3 \times 10^5$ . The typical condensate fraction and cloud temperature were 0.6 and 130 nK, respectively. We applied a bias magnetic field  $\vec{B}$  ( $\parallel \hat{x}$ ) of approximately  $14 \mu\text{T}$ . The angle  $\alpha$  between the probe polarization plane and  $\vec{B}$  was chosen to be around the magic angle of  $54.7^\circ$  to minimize light-induced nonlinear spin evolution [27–29].

Figure 2(a) shows a typical set of contrast images taken by 35 probe pulses. The color represents the contrast  $I/I_0$ , where  $I$  and  $I_0$  are the probe intensities on the camera with and without atoms, respectively. The spin state of the BEC was initially polarized along  $\vec{B}$  and rotated onto the  $y$ - $z$  plane by an rf  $\pi/2$  pulse. The magnetic field components along  $y$  and  $z$  were nulled within 100 nT uncertainty using rf spectroscopy by absorption imaging with the Stern-Gerlach technique. We performed fine adjustment of the rf frequency and pulse length to maximize the precession signal amplitude in the TPPCI. After a time  $t_0$ , the BEC was imaged with probe pulses evenly spaced by  $\Delta t$ . The probe-pulse width  $\tau_p$  was less than  $1 \mu\text{s}$ , which was sufficiently shorter than the Larmor period  $\tau_L = 2\pi\hbar/(g\mu_B|\vec{B}|) \sim 10 \mu\text{s}$ . Here  $\hbar$  is the reduced Planck constant,  $g$  is the Landé  $g$  factor, and  $\mu_B$  is the Bohr magneton. The temporal oscillation in the contrast signal in each region reflects the spin precession, aliased by the sampling rate. When the atomic spin points toward the  $\pm z$  axis, atoms interact with only one circular polarization component, as illustrated in Fig. 1(c), and the contrast signal appears on either region.

The contrast is related to phase shifts of the probe caused by the atoms (see Supplemental Material [30] for details).

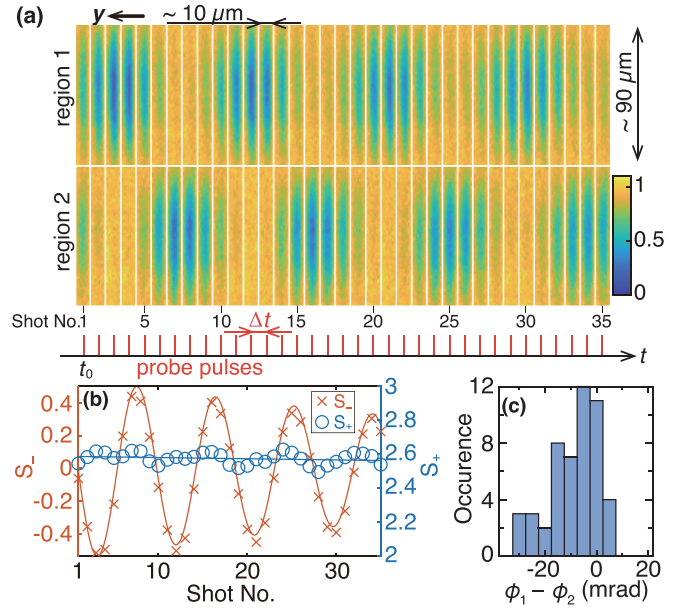


FIG. 2. (a) Typical set of contrast images. The top and bottom rows display the orthogonal polarization components and are sorted by time from left to right. The color bar represents the contrast. (b) Difference ( $S_-$ ) and sum ( $S_+$ ) signals. The lines are fits to the data. (c) Histogram of  $\phi_1 - \phi_2$  over 50 experimental runs. The data is taken with  $t_0 = 0.1 \text{ ms}$ ,  $\Delta t = 30 \mu\text{s}$ ,  $\tau_p = 0.60 \mu\text{s}$ , photon fluence per pulse of  $8.3 \times 10^3 \mu\text{m}^{-2}$ , and  $\Delta = -1.537 \text{ GHz}$ .

When the phase shifts are sufficiently smaller than unity, the sum and difference of the contrasts at the two regions are approximated as

$$s_+(x, y) = 2 - 4(\varphi + \theta_1 \cos 2\alpha + \theta_2 \sin 2\alpha) \quad (1)$$

and

$$s_-(x, y) = 4\theta_3, \quad (2)$$

respectively. Here,  $\varphi$  is the polarization-independent phase shift, and  $\theta_i$  are the polarization-dependent shifts.  $\theta_{1,2}$  are related to the atomic birefringence and spin alignment (second-rank polarization moment). As  $\theta_3$  originates from the optical activity and is proportional to  $\langle F_z \rangle$ ,  $s_-$  is a direct measure of  $\langle F_z \rangle$  within the small phase shift approximation.

With TPPCI,  $\langle F_z \rangle$  and the number of atoms can be tracked separately, as shown below, whereas both the spin state and atom number contribute to the signal in other similar imaging methods such as spin-sensitive PCI [18,33], and dual-port Faraday imaging [34]. TPPCI is immune to probe-intensity fluctuation, due to the balanced configuration. The linearly polarized probe eliminates the systematic error due to the vector shift by a circularly polarized probe [18]. TPPCI is a powerful tool for loss measurement and magnetometry as demonstrated here, as well as for the study of the spatial magnetic properties in a dissipative open system [35] and exotic spin states.

For a qualitative analysis, we integrated  $s_{\pm}$  over a region of interest (ROI) around the center of the BEC. We show the integrated signals,  $S_+$  and  $S_-$ , in Fig. 2(b). The observed gradual damping of  $S_-$  was ascribed to atom loss and spin decoherence due to the probe pulses. The loss of atoms also

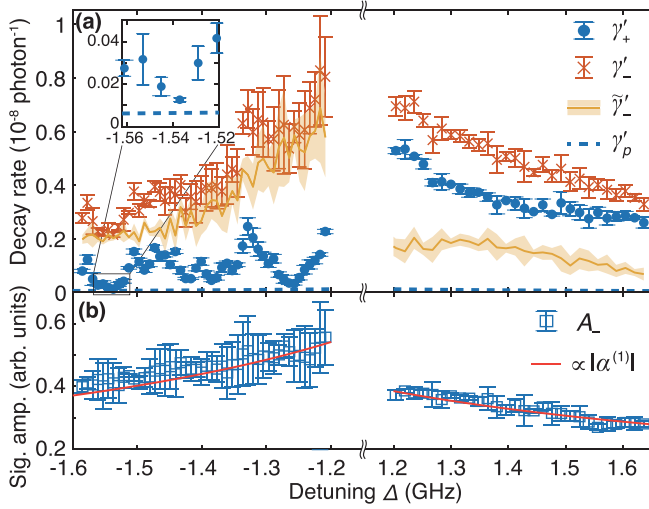


FIG. 3. Detuning dependence of the sum and precession signals. (a) Normalized decay rates.  $\gamma'_+$ ,  $\gamma'_-$ , and  $\tilde{\gamma}'_-$  are plotted as a function of  $\Delta$ . The dotted line represents the photon scattering rate  $\gamma'_p$ . (b) Precession signal amplitude. The solid lines are a fit based on the theoretical frequency dependence.

resulted in the gradual decrease of  $S_+$  through  $\phi$ . The small oscillation in  $S_+$  was attributed to the contribution from the spin alignment, in addition to misalignment in the probe system. The slight increase of the oscillation amplitude suggests that nonlinear spin evolution was induced by the probe light. We note that the phase shifts were so substantial that Eqs. (1) and (2) were not perfectly valid. In the data analysis, we calculated the polarization rotation angle  $\gamma$  as a more appropriate measure of  $\langle F_z \rangle$  (see Supplemental Material [30]), instead of subtracting of the signals at the two ROIs.

### III. RESULTS

#### A. Atom loss and signal decay

We investigated the atom loss and the decay of the precession amplitude as a function of  $\Delta$ .  $S_+$  was fitted with  $A_+ \exp[-\gamma_+(t - t_0)]$  to estimate the atom loss rate  $\gamma_+$ . We also fitted the precession signal with  $A_- \exp[-\gamma_-(t - t_0)] \sin[\omega(t - t_0) + \phi_0]$ , where  $\gamma_-$  is the decay rate of the precession amplitude,  $\phi_0$  is the precession phase at  $t = t_0$ , and  $\omega$  is the aliased precession frequency. The fitting models adopted here are valid while nonexponential decay due to multibody losses and nonlinear spin evolution are sufficiently small.

The frequency dependencies of normalized atom loss and precession decay rates,  $\gamma'_+$  and  $\gamma'_-$ , are shown in Fig. 3(a). Here,  $\gamma'_+ = \gamma_+/N_p$  and  $\gamma'_- = \gamma_-/N_p$ , where  $N_p$  is the number of photons per pulse passing through the ROI. The red- and blue-detuned sides of the frequency dependencies were independently measured, and the experimental conditions, such as the environmental magnetic field and the optical trap depth, were slightly different. The total photon fluences  $\Phi_p$  for the red- and blue-detuned sides were  $5.3 \times 10^5 \mu\text{m}^{-2}$  and  $4.5 \times 10^5 \mu\text{m}^{-2}$ , respectively. It was found that  $\gamma'_+$  was asymmetric with respect to the sign of  $\Delta$ . The asymmetry in  $\gamma'_+$  suggests that the atom loss was mainly induced by light-assisted collisions [21–23,25], the rate of which as a

function of optical frequency is smooth for blue-detuned light, but is expected to show discrete peaks for red-detuned light. The dotted line in Fig. 3(a) shows the photon-scattering rate divided by  $N_p$ ,  $\gamma'_p$ . The normalized atom loss rate  $\gamma'_+$  was close to  $\gamma'_p$  around  $\Delta = -1.537$  GHz, as shown in the inset.

The net decay rate of the Larmor precession,  $\tilde{\gamma}'_- = \gamma'_- - \gamma'_+$ , showed little discrete dependence on  $\Delta$ .  $\tilde{\gamma}'_-$  is represented by the solid line with an error band in Fig. 3(a). Although the threshold to the Rayleigh superradiant scattering was independently measured to be  $\Phi_p \sim 4 \times 10^5 \mu\text{m}^{-2}$  for  $\Delta = -1.257$  GHz, the observed  $\tilde{\gamma}'_-$  roughly agrees with a numerical simulation with no superradiance. This implies that the nonlinear spin evolution is a dominant source of  $\tilde{\gamma}'_-$  in our configuration. The nonlinear spin evolution may be suppressed with a multicolor probe [36,37] or with the two-polarization decoupling technique for measurement of specific spin variables [38], the latter of which can be used for magnetometry with nonlinear magneto-optical rotation.

The amplitude  $A_-$  had a monotonic detuning dependence regardless of the sign of the detuning, as plotted in Fig. 3(b). The dependence is in good agreement with the theoretical expectation, which is proportional to the absolute value of the vector polarizability  $\alpha^{(1)} \propto 3/(\Delta + \omega_{\text{hfs}}/2) + 1/(\Delta - \omega_{\text{hfs}}/2)$  [39,40], where  $\omega_{\text{hfs}} = 2\pi \times 814.5$  MHz is the hyperfine splitting in the excited  $P_{1/2}$  states. Since noise sources such as optical and atomic spin shot noises are usually independent of the probe frequency, the signal-to-noise ratio is maximized at the red-detuned side.

#### B. Phase sensitivity

We evaluated the precession phase sensitivity  $\delta\phi$  for  $\Delta = -1.537$  GHz, which gave a small signal decay rate, and  $\Phi_p = 4.1 \times 10^5 \mu\text{m}^{-2}$ .  $t_0$  was fixed to 0.1 ms in this evaluation. To avoid the effect of the common magnetic field fluctuation, including an ac line noise of  $< 1$  nT at 50 Hz measured by a spin echo method [19], we applied two ROIs around the atom cloud center. We obtained  $\phi_0$  in each ROI, hereafter denoted as  $\phi_1$  and  $\phi_2$ , from the damped-oscillation fitting. By taking the difference,  $\phi_1 - \phi_2$ , the contribution of the common field fluctuation can be removed. Assuming the correlation between  $\phi_1$  and  $\phi_2$  was negligible, the phase sensitivity  $\delta\phi$  was evaluated by  $\delta\phi = \sqrt{\text{Var}[\phi_1 - \phi_2]}/2$ .

We obtained  $\delta\phi$  and  $A_-$  with varying the separation between the two ROIs of  $1.4 \times 10^2 \mu\text{m}^2$  ( $5.3 \mu\text{m}$  in the  $y$  direction and  $27 \mu\text{m}$  in the  $x$  direction). The ROIs were arranged along the  $x$  axis and symmetrically placed with respect to the BEC center. The separation was set to be  $\geq 5.3 \mu\text{m}$ . As the estimated imaging resolution (Rayleigh's criterion) is about  $3 \mu\text{m}$  and the spin healing length at the cloud center is about  $3 \mu\text{m}$ ,  $\phi_1$  and  $\phi_2$  are expected to be independent for the separation  $\geq 5.3 \mu\text{m}$ . The obtained  $\delta\phi$  as a function of the separation is shown in Fig. 4(a). The corresponding histogram for the separation of  $5.3 \mu\text{m}$  is shown in Fig. 2(c). The increase in  $\delta\phi$  for larger separation is due to the decrease in the atomic density. The precession amplitude  $A_-$  (averaged over the two ROIs) is shown in Fig. 4(b). Because the spin was almost perfectly stretched for  $t_0 = 0.1$  ms,  $A_-$  was proportional to the number of atoms in a single ROI,  $N_a$ .

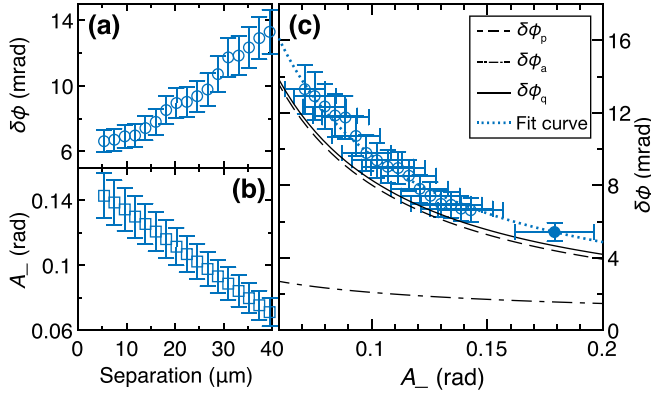


FIG. 4. Phase noise analysis. Separation dependencies of (a) phase sensitivity and (b) precession amplitude. The error bars indicate standard deviations over 50 experimental runs. (c) Precession amplitude dependence of phase sensitivity. The open and filled circles represent measured data and  $\delta\phi_c$ , respectively. The dashed, dash-dotted, and solid lines show the phase uncertainties due to the atomic, optical, and total quantum noises, respectively. The dotted line shows a fitted noise model including a technical noise. The data was taken with  $t_0 = 0.1$  ms,  $\tau_p = 0.60$   $\mu\text{s}$ ,  $\Delta t = 30$   $\mu\text{s}$ ,  $\Delta = -1.537$  GHz, and  $\Phi_p = 4.1 \times 10^5$   $\mu\text{m}^{-2}$ .

We plotted  $\delta\phi$  as a function of  $A_-$  in Fig. 4(c) (open circles). The estimated phase uncertainties,  $\delta\phi_a$  and  $\delta\phi_p$ , due to the atomic spin and optical shot noises, respectively, are also plotted.  $\delta\phi_a$  is given by  $1/(2\sqrt{N_a})$  for a stretched (coherent) spin state. In the estimation,  $N_a$  was calculated from the density profile and the total atom number of the BEC. The photon shot noise results in the uncertainty in the phase estimation by a sinusoidal fitting approximately given by  $\delta\phi_p = 2\sqrt{2}\sigma/(A_- \sqrt{N_s})$  [41], where  $N_s$  is the number of imaging shots and  $\sigma \propto \sqrt{N_s}/\Phi_p$  is the fluctuation in the probe polarization detection due to the photon shot noise in each shot. The solid line in Fig. 4(c) is the total quantum noise contribution,  $\delta\phi_q = \sqrt{\delta\phi_a^2 + \delta\phi_p^2}$ , indicating the quantum noises were dominant in  $\delta\phi$ . The phase sensitivity for the short separation was comparable to the previous record for a BEC magnetometer (10 mrad over 120  $\mu\text{m}^2$ ) [18]. We modeled the noise in the phase estimation as  $\sqrt{\delta\phi_a^2 + \delta\phi_p^2 + \delta\phi_{\text{tech}}^2}$ , where  $\delta\phi_{\text{tech}} = 2\sqrt{2}\sigma_{\text{tech}}/(A_- \sqrt{N_s})$  is the phase uncertainty due to the technical fluctuation  $\sigma_{\text{tech}}$  in the probe polarization aside from the quantum noises. The data was well fitted by this model with  $\sigma_{\text{tech}}$  being the fitting parameter. The fitted value of  $\sigma_{\text{tech}}$  was 1.03(4) mrad. We estimated a phase sensitivity at the BEC center,  $\delta\phi_c$ , based on the fitted noise model. Using a ROI of  $1.4 \times 10^2$   $\mu\text{m}^2$  at the BEC center for the same data above, the precession amplitude was measured to be 0.18(2) rad. We obtained  $\delta\phi_c = 5.4(6)$  mrad by extrapolating the fit [see filled circle in Fig. 4(c)].

### C. Magnetic field sensitivity

We also evaluated the magnetic field sensitivity,  $\delta B \sqrt{T_{\text{cycle}}} = \hbar \delta\phi \sqrt{T_{\text{cycle}}}/(g\mu_B t_0)$ , where  $T_{\text{cycle}}$  is the cycle time of a single measurement run including the time taken for loading atoms into a magneto-optical trap.  $T_{\text{cycle}}$  was fixed to 60 s in our experiment regardless of the value of  $t_0$ . We found

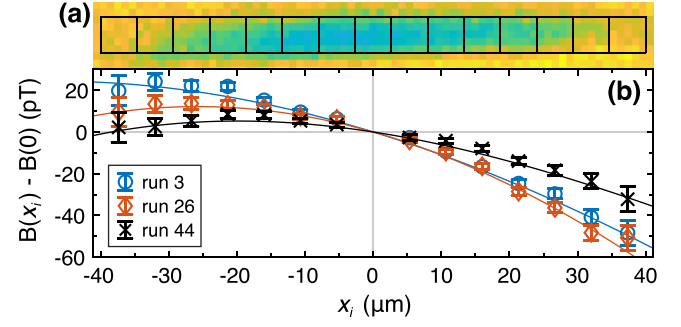


FIG. 5. Measurement of a magnetic field profile. (a) Typical contrast image of the BEC with  $t_0 = 300$  ms. Multiple ROIs of  $28 \mu\text{m}^2$  are indicated by the rectangles. (b)  $B(x_i)$  for different experimental runs. The solid lines are the fitted curves with a third-order polynomial function.

that a  $t_0$  around 300 ms was optimal for attaining a good field sensitivity. The optimal time was close to the  $1/e$ -decay time  $T_-$  of the precession amplitude under no probe light (before  $t_0$ ), which was measured to be  $T_- = 0.57 \pm 0.03$  s. We note that  $A_-$  monotonically decreased, in contrast to the case of the spinor BEC in the lower hyperfine state  $F = 1$ , where signal modulation occurs due to a quadratic Zeeman shift [14]. The monotonic decay should be related to the inelastic collisions [35].

The magnetic field sensitivity was estimated to be  $\delta B \sqrt{T_{\text{cycle}}} = 5.0(4)$  pT/ $\sqrt{\text{Hz}}$  using a ROI of  $1.4 \times 10^2$   $\mu\text{m}^2$  ( $5.3 \mu\text{m} \times 27 \mu\text{m}$ ) at the BEC center with  $t_0 = 300$  ms,  $\Delta = -1.537$  GHz, and  $\Phi_p = 3.9 \times 10^5$   $\mu\text{m}^2$ . In this estimation,  $\delta\phi = 8.5(6)$  mrad was estimated based on the fitted noise model shown in Fig. 4(c) using the measured precession amplitude  $A_- = 0.116(8)$  rad. We note that the stretched spin state was maintained under the reduced magnetic field gradient for the best magnetometry performance [42] and the noise model should hold for  $t_0 = 300$  ms. This estimation gives the field sensitivity over the ROI of  $5.3 \mu\text{m} \times 27 \mu\text{m}$  assuming that transport of spin, for example, due to spin diffusion [43] is negligible compared with the ROI size. The estimated field sensitivity for a given spatial resolution is better than the reported sensitivities for previous BEC magnetometers [14,16,18,19,44]. This indicates the effectiveness of the probe optimization.

We calculated the one-dimensional local field  $B(x_i)$  from  $B(x_i) = \hbar \langle \phi_0(x) \rangle / (g\mu_B t_0)$ , where  $\phi_0(x)$  represents the local precession phase at  $t = t_0$  and its expectation value  $\langle \phi_0(x) \rangle$  was taken over a ROI of  $28 \mu\text{m}^2$  around  $x_i$ . The ROIs for the analysis are shown in Fig. 5(a). We note that the magnetic features of short length scales may not be detected faithfully due to spin diffusion [43]. If the spin diffused across the present ROI of  $28 \mu\text{m}^2$  and the spatial resolution became worse than the ROI size, the analysis here corresponds to spatial oversampling and we could not resolve magnetic field features smaller than the spatial resolution.

The measured local fields  $B(x_i)$  [with respect to  $B(0)$ ] for different experimental runs are plotted in Fig. 5(b). The error bars were estimated from the above-mentioned noise model for the ROI size of  $28 \mu\text{m}^2$ . We fitted the measured

field profile with a third-order polynomial function. The fitted curves are represented by the solid lines in Fig. 5(b). The estimated field gradient and half-width of its  $1\sigma$  confidence interval, for example, in run 3, were computed to be  $-0.84$  and  $0.06$  pT/ $\mu\text{m}$ , under the assumption of spatially slowly varying field. The observed shot-to-shot variation in the field profiles may be partly due to fluctuation in the fictitious magnetic field induced by the trapping beams [42].

#### IV. DISCUSSIONS

Our technique can be combined with other practically feasible improvements to obtain a better sensitivity. As we operated the magnetometer with a low duty cycle of  $5 \times 10^{-3}$ , the field sensitivity can be greatly improved by the fast production of a BEC [25,45,46] or extending the free-precessing time using a spatially single-mode BEC of long spin coherence time [14,15]. For ac field detection, bang-bang control is also useful [47]. Suppression of the nonlinear spin evolution, as discussed in Sec. III A, can also lead to the increase in the probe fluence and therefore improve the sensitivity. In addition, the selection of the probe detuning is important, but further investigation of the effects of the probe-induced loss, nonlinear spin evolution, and photon scattering on the sensitivity is required to identify the optimum probe detuning.

The reduction in the photon shot noise contribution demonstrated here by increasing the probe fluence opens the possibility for significant spin squeezing in a BEC via QND measurement. Our spin measurement is equivalent to Faraday polarization rotation detection, in which Faraday (vector) atom-light interaction fulfills the criteria of a QND measurement of the spin component along the probe axis [48,49]. The spin squeezing via the measurement and reduction of the spin shot noise conditioned to the readout result are expected. The increased probe strength is beneficial for achieving high squeezing level, because the strong probe makes greater quantum correlation between the atoms and light. As a result of

the increased probe strength, the spin shot noise contribution becomes more dominant and the spin squeezing will be of particular importance in further sensitivity enhancement.

We evaluated the energy resolution, a figure of merit of a spatially resolved magnetometry, given by  $\delta B^2 T_{\text{cycle}} V / (2\mu_0)$ , where  $V$  is the measurement volume and  $\mu_0$  is the vacuum permeability. The evaluated value was  $8 \times 10 \hbar$  for atoms in the area of  $140 \mu\text{m}^2$  used in sensitivity analysis. This is better than that for diamond sensors using spin ensembles [50] and comparable to reported values for SQUIDs [51–53] at low frequency and for the most sensitive atomic magnetometer [8]. The *essential* energy resolution with a full duty cycle was  $0.4\hbar$ , surpassing the limitation of SQUIDs  $\approx \hbar$  [54,55]. This suggests that a spinor BEC can be a strong candidate for sensitive magnetometry with micrometer resolution. It should be noted that spin diffusion is neglected in this evaluation. We expect sensitive magnetometry with a better spatial resolution will be realized by adding confinement potential.

#### V. CONCLUSIONS

In conclusion, we realized sensitive spatially resolved magnetometry using a BEC with a bright probe. We investigated probe-induced losses in the atom number and magnetization to find that the atom loss was suppressed at a well-tuned probe frequency. Our result is a significant step toward realizing ultrasensitive spatially resolved BEC magnetometers and achieving unprecedented magnetic field sensitivity with a micrometer-scale spatial resolution, which is of fundamental and practical interest.

#### ACKNOWLEDGMENTS

This work was supported by MEXT Quantum Leap Flagship Program (MEXT Q-LEAP) Grant No. JPMXS0118070326.

N.S. and K.S. contributed equally to this work.

- 
- [1] M. S. Safronova, D. Budker, D. DeMille, Derek F. Jackson Kimball, A. Derevianko, and C. W. Clark, *Rev. Mod. Phys.* **90**, 025008 (2018).
  - [2] Y. Hu, G. Z. Iwata, M. Mohammadi, E. V. Sillella, A. Wickenbrock, J. W. Blanchard, D. Budker, and A. Jerschow, *Proc. Natl. Acad. Sci. USA* **117**, 10667 (2020).
  - [3] N. Aslam, M. Pfender, P. Neumann, R. Reuter, A. Zappe, F. Fávoro de Oliveira, A. Denisenko, H. Sumiya, S. Onoda, J. Isoya, and J. Wrachtrup, *Science* **357**, 67 (2017).
  - [4] M. Hämmäläinen, R. Hari, R. J. Ilmoniemi, J. Knuutila, and O. V. Lounasmaa, *Rev. Mod. Phys.* **65**, 413 (1993).
  - [5] E. Boto, N. Holmes, J. Leggett, G. Roberts, V. Shah, S. S. Meyer, L. D. Muñoz, K. J. Mullinger, T. M. Tierney, S. Bestmann, G. R. Barnes, R. Bowtell, and M. J. Brookes, *Nature (London)* **555**, 657 (2018).
  - [6] R. M. Hill, E. Boto, N. Holmes, C. Hartley, Z. A. Seedat, J. Leggett, G. Roberts, V. Shah, T. M. Tierney, M. W. Woolrich, C. J. Stagg, G. R. Barnes, R. Bowtell, R. Slater, and M. J. Brookes, *Nat. Commun.* **10**, 4785 (2019).
  - [7] I. K. Kominis, T. W. Kornack, J. C. Allred, and M. V. Romalis, *Nature (London)* **422**, 596 (2003).
  - [8] H. B. Dang, A. C. Maloof, and M. V. Romalis, *Appl. Phys. Lett.* **97**, 151110 (2010).
  - [9] M. Schmelz, R. Stolz, V. Zakosarenko, T. Schönau, S. Anders, L. Fritzsche, M. Mück, and H.-G. Meyer, *Supercond. Sci. Technol.* **24**, 065009 (2011).
  - [10] I. Baumgart, J.-M. Cai, A. Retzker, M. B. Plenio, and C. Wunderlich, *Phys. Rev. Lett.* **116**, 240801 (2016).
  - [11] G. Balasubramanian, P. Neumann, D. Twitchen, M. Markham, R. Kolesov, N. Mizuochi, J. Isoya, J. Achard, J. Beck, J. Tissler, V. Jacques, P. R. Hemmer, F. Jelezko, and J. Wrachtrup, *Nat. Mater.* **8**, 383 (2009).
  - [12] O. Elfasson, R. Heck, J. S. Laustsen, M. Napolitano, R. Müller, M. G. Bason, J. J. Arlt, and J. F. Sherson, *J. Phys. B: At., Mol. Opt. Phys.* **52**, 075003 (2019).

- [13] M. W. Mitchell and S. Palacios Alvarez, *Rev. Mod. Phys.* **92**, 021001 (2020).
- [14] M. Jasperse, M. J. Kewming, S. N. Fischer, P. Pakkiam, R. P. Anderson, and L. D. Turner, *Phys. Rev. A* **96**, 063402 (2017).
- [15] S. Palacios, S. Coop, P. Gomez, T. Vanderbruggen, Y. N. Martinez de Escobar, M. Jasperse, and M. W. Mitchell, *New J. Phys.* **20**, 053008 (2018).
- [16] S. Wildermuth, S. Hofferberth, I. Lesanovsky, E. Haller, L. M. Andersson, S. Groth, I. Bar-Joseph, P. Krüger, and J. Schmiedmayer, *Nature (London)* **435**, 440 (2005).
- [17] F. Yang, S. F. Taylor, S. D. Edkins, J. C. Palmstrom, I. R. Fisher, and B. L. Lev, *Nat. Phys.* **16**, 514 (2020).
- [18] M. Vengalattore, J. M. Higbie, S. R. Leslie, J. Guzman, L. E. Sadler, and D. M. Stamper-Kurn, *Phys. Rev. Lett.* **98**, 200801 (2007).
- [19] Y. Eto, H. Ikeda, H. Suzuki, S. Hasegawa, Y. Tomiyama, S. Sekine, M. Sadgrove, and T. Hirano, *Phys. Rev. A* **88**, 031602(R) (2013).
- [20] M. Auzinsh, D. Budker, D. F. Kimball, S. M. Rochester, J. E. Stalnaker, A. O. Sushkov, and V. V. Yashchuk, *Phys. Rev. Lett.* **93**, 173002 (2004).
- [21] K. Burnett, P. S. Julienne, and K.-A. Suominen, *Phys. Rev. Lett.* **77**, 1416 (1996).
- [22] A. Fuhrmanek, R. Bourgain, Y. R. P. Sortais, and A. Browaeys, *Phys. Rev. A* **85**, 062708 (2012).
- [23] H. Jelassi and L. Pruvost, *Phys. Rev. A* **89**, 032514 (2014).
- [24] J. Hu, A. Urvoy, Z. Vendeiro, V. Crépel, W. Chen, and V. Vuletić, *Science* **358**, 1078 (2017).
- [25] A. Urvoy, Z. Vendeiro, J. Ramette, A. Adiyatullin, and V. Vuletić, *Phys. Rev. Lett.* **122**, 203202 (2019).
- [26] T. Kuwamoto, K. Araki, T. Eno, and T. Hirano, *Phys. Rev. A* **69**, 063604 (2004).
- [27] G. A. Smith, S. Chaudhury, A. Silberfarb, I. H. Deutsch, and P. S. Jessen, *Phys. Rev. Lett.* **93**, 163602 (2004).
- [28] I. H. Deutsch and P. S. Jessen, *Opt. Commun.* **283**, 681 (2010).
- [29] G. Colangelo, R. J. Sewell, N. Behbood, F. M. Ciurana, G. Triginer, and M. W. Mitchell, *New J. Phys.* **15**, 103007 (2013).
- [30] See Supplemental Material at <http://link.aps.org/supplemental/10.1103/PhysRevA.104.L041306> for further details of signals in TPPCI, which includes Refs. [31,32].
- [31] A. Yariv and P. Yeh, *Photonics: Optical Electronics in Modern Communications*, 6th ed. (Oxford University Press, New York, 2007).
- [32] D. M. Stamper-Kurn and M. Ueda, *Rev. Mod. Phys.* **85**, 1191 (2013).
- [33] J. M. Higbie, L. E. Sadler, S. Inouye, A. P. Chikkatur, S. R. Leslie, K. L. Moore, V. Savalli, and D. M. Stamper-Kurn, *Phys. Rev. Lett.* **95**, 050401 (2005).
- [34] F. Kaminski, N. S. Kampel, M. P. H. Steenstrup, A. Griesmaier, E. S. Polzik, and J. H. Müller, *Eur. Phys. J. D* **66**, 227 (2012).
- [35] Y. Eto, H. Shibayama, K. Shibata, A. Torii, K. Nabeta, H. Saito, and T. Hirano, *Phys. Rev. Lett.* **122**, 245301 (2019).
- [36] M. Saffman, D. Oblak, J. Appel, and E. S. Polzik, *Phys. Rev. A* **79**, 023831 (2009).
- [37] J. Appel, P. J. Windpassinger, D. Oblak, U. B. Hoff, N. Kjaergaard, and E. S. Polzik, *Proc. Natl. Acad. Sci. USA* **106**, 10960 (2009).
- [38] M. Koschorreck, M. Napolitano, B. Dubost, and M. W. Mitchell, *Phys. Rev. Lett.* **105**, 093602 (2010).
- [39] J. M. Geremia, J. K. Stockton, and H. Mabuchi, *Phys. Rev. A* **73**, 042112 (2006).
- [40] S. Jammi, T. Pyragius, M. G. Bason, H. M. Florez, and T. Fernholz, *Phys. Rev. A* **97**, 043416 (2018).
- [41] S. M. Kay, *Fundamentals of Statistical Signal Processing: Estimation Theory*, 1st ed. (Prentice-Hall, Englewood Cliffs, NJ, 1993).
- [42] K. Shibata, N. Sekiguchi, and T. Hirano, *Phys. Rev. A* **103**, 043335 (2021).
- [43] G. E. Marti, A. MacRae, R. Olf, S. Lourette, F. Fang, and D. M. Stamper-Kurn, *Phys. Rev. Lett.* **113**, 155302 (2014).
- [44] W. Muessel, H. Strobel, D. Linnemann, D. B. Hume, and M. K. Oberthaler, *Phys. Rev. Lett.* **113**, 103004 (2014).
- [45] R. Roy, A. Green, R. Bowler, and S. Gupta, *Phys. Rev. A* **93**, 043403 (2016).
- [46] K. Yamashita, K. Hanasaki, A. Ando, M. Takahama, and T. Kinoshita, *Phys. Rev. A* **95**, 013609 (2017).
- [47] Y. Eto, M. Sadgrove, S. Hasegawa, H. Saito, and T. Hirano, *Phys. Rev. A* **90**, 013626 (2014).
- [48] A. Kuzmich, N. P. Bigelow, and L. Mandel, *Europhys. Lett.* **42**, 481 (1998).
- [49] Y. Takahashi, K. Honda, N. Tanaka, K. Toyoda, K. Ishikawa, and T. Yabuzaki, *Phys. Rev. A* **60**, 4974 (1999).
- [50] T. Wolf, P. Neumann, K. Nakamura, H. Sumiya, T. Ohshima, J. Isoya, and J. Wrachtrup, *Phys. Rev. X* **5**, 041001 (2015).
- [51] R. T. Wakai and D. J. Van Harlingen, *Appl. Phys. Lett.* **52**, 1182 (1988).
- [52] D. D. Awschalom, J. R. Rozen, M. B. Ketchen, W. J. Gallagher, A. W. Kleinsasser, R. L. Sandstrom, and B. Bumble, *Appl. Phys. Lett.* **53**, 2108 (1988).
- [53] M. Schmelz, V. Zakosarenko, T. Schönau, S. Anders, S. Linzen, R. Stolz, and H. G. Meyer, *Supercond. Sci. Technol.* **30**, 014001 (2017).
- [54] R. H. Koch, D. J. Van Harlingen, and J. Clarke, *Phys. Rev. Lett.* **45**, 2132 (1980).
- [55] R. H. Koch, D. J. Van Harlingen, and J. Clarke, *Appl. Phys. Lett.* **38**, 380 (1981).